

A High-Sensitivity Lanthanide Nanoparticle Reporter for Mass Cytometry: Tests on Microgels as a Proxy for Cells

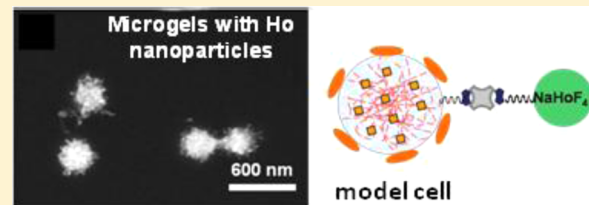
Wanjuan Lin,[†] Yi Hou,[†] Yijie Lu,[†] Ahmed I. Abdelrahman,[†] Pengpeng Cao,[†] Guangyao Zhao,[†] Lemuel Tong,[†] Jieshu Qian,[†] Vladimir Baranov,[‡] Mark Nitz,[†] and Mitchell A. Winnik*,[†]

[†]Department of Chemistry, University of Toronto, 80 St. George Street, Toronto, Ontario, Canada M5S 3H6

[‡]DVS Sciences, 70 Esna Park Drive, Markham, Ontario, Canada L3R 6E7

Supporting Information

ABSTRACT: This paper addresses the question of whether one can use lanthanide nanoparticles (e.g., NaHoF₄) to detect surface biomarkers expressed at low levels by mass cytometry. To avoid many of the complications of experiments on live or fixed cells, we carried out proof-of-concept experiments using aqueous microgels with a diameter on the order of 700 nm as a proxy for cells. These microgels were used to test whether nanoparticle (NP) reagents would allow the detection of as few as 100 proteins per “cell” in cell-by-cell assays. Streptavidin (SAv), which served as the model biomarker, was attached to the microgel in two different ways. Covalent coupling to surface carboxyls of the microgel led to large numbers ($>10^4$) of proteins per microgel, whereas biotinylation of the microgel followed by exposure to SAv led to much smaller numbers of SAv per microgel. Using mass cytometry, we compared two biotin-containing reagents, which recognized and bound to the SAvs on the microgel. One was a metal chelating polymer (MCP), a biotin end-capped polyaspartamide containing 50 Tb³⁺ ions per probe. The other was a biotinylated NaHoF₄ NP containing 15 000 Ho atoms per probe. Nonspecific binding was determined with bovine serum albumin (BSA) conjugated microgels. The MCP was effective at detecting and quantifying SAvs on the microgel with covalently bound SAv (20 000 SAvs per microgel) but was unable to give a meaningful signal above that of the BSA-coated microgel for the samples with low levels of SAv. Here the NP reagent gave a signal 2 orders of magnitude stronger than that of the MCP and allowed detection of NPs ranging from 100 to 500 per microgel. Sensitivity was limited by the level of nonspecific adsorption. This proof of concept experiment demonstrates the enhanced sensitivity possible with NP reagents in cell-by-cell assays by mass cytometry.



INTRODUCTION

One of the goals of modern bioanalytical chemistry is the simultaneous (multiplexed) detection of multiple biomarkers in individual cells. Biomarkers are defined as characteristic proteins, genes, or small molecules that can be measured and evaluated as indicators of normal biological or pathogenic processes.¹ In flow cytometry, bioaffinity agents are labeled with fluorescent dyes or quantum dots (QDs) to allow rapid cell-by-cell analysis of multiple biomarkers. One of the limitations of flow cytometry is the breadth of the emission bands of the luminescent species used as antibody (Ab) labels. The spillover of overlapping emissions requires compensation and restricts the number of species that can be detected simultaneously for each cell. The Roederer group has shown that 18-color flow cytometry is possible,² but this level of multiplexing is not routine.

Mass cytometry is a new technique designed to address the challenges of polychromatic flow cytometry by replacing fluorophores with stable heavy metal isotopes as Ab tags.³ In this technique, cells are introduced individually but stochastically into the plasma torch of an inductively coupled plasma mass spectrometer (ICP-MS) equipped with time-of-flight detection. Each Ab is labeled with a specific metal isotope, and

the multiplexing capability comes from instrument's ability to resolve metal ions that differ in mass by a single atomic mass unit. To achieve a signal strong enough for detection by ICP-MS, Abs have to be labeled with multiple copies of a metal isotope. This has been accomplished with metal-chelating polymers (MCPs) with 30–80 pendant chelating groups and appropriate end group functionality.^{4–6} Abs labeled with these polymers typically carry 150–250 metal atoms per Ab.⁶ Ln ions are attractive for mass cytometry because of their low natural abundance, similar chemistry, and the availability of isotopically enriched samples.

The strength of mass cytometry is the multiparameter capability.⁷ For example, the Nolan group examined regulatory cell signaling behavior across hematopoietic cells using two 34-parameter panels that included 31 antibody targets, a DNA intercalator, and measures of viability and cell size.⁸ Newell et al.⁹ reported a 37-parameter study of virus-specific T cell function and phenotype, and a more recent paper described T-cell experiments with 109 multiplexed tetramers plus 23

Received: September 20, 2013

Revised: February 24, 2014

Published: March 11, 2014



antibody channels.¹⁰ Sample throughput can be further enhanced with mass-tag cellular barcoding, analogous to fluorescent cell barcoding.¹¹ On the other hand, mass cytometry lacks sensitivity compared to fluorescence detection. Cellular protein expression levels range from a few copies to 10^7 copies per cell,¹² and many important proteins, such as cytokine receptors, are expressed at levels too low to detect easily, even by fluorescence.¹³ While there are no publications describing the lower limits of biomarker detection by mass cytometry, a recent paper reported experiments using an MCP reagent to generate ca. 200 metal ions per Ab. The authors could detect and quantify target biomarkers with abundances in the range of 10^4 – 10^7 per cell.⁶ The goal of this work is to demonstrate that by using NaLnF_4 nanoparticle reagents⁷ in the place of MCPs, it will be possible to detect much smaller numbers of a particular biomarker per cell than is possible with MCP reagents.¹⁴

Signal strength for ICP-MS increases linearly with the number of metal ions of a particular isotope. Thus, if one could attach 10 000 metal atoms per antibody, one might be able to increase the sensitivity by a factor of 500 and detect as few as 100 copies of a particular biomarker per cell. Many types of NPs with a 10 nm diameter (the dimensions of an IgG antibody) contain on the order of 8000–10 000 metal atoms.¹⁵ QDs containing Cd, Se, and Te can be detected by mass cytometry but are not large enough to provide a substantial gains in signal.¹⁶ The most attractive candidates for mass cytometry are NPs related to Ln-doped NaYF_4 , which are being developed for optical up-conversion¹⁷ and NaGdF_4 ,¹⁸ which are being developed as magnetic resonance imaging contrast agents.

While the characteristics of a NP are determined by the composition of its core, the coating plays an essential role in bioanalytical applications. The coating must provide colloidal stability in aqueous media, prevent aggregation, provide functional groups for bioconjugation, and suppress nonspecific adsorption. Satisfying all of these criteria is a daunting task. Not only is the *in vitro* and *in vivo* performance of nanoparticles dependent on the size, charge, hydrophilicity, and flexibility of the coating molecules, but the number, density, and type of reactive functionality on the NP surface regulate the interactions between nanoparticles and their targets.¹⁹ In addition, there is the difficulty of separating Ab-NP conjugates from excess NPs used in the conjugation reaction.²⁰ Finally, there is the ubiquitous problem of nonspecific interactions. For a reagent to be useful in a targeted assay, it not only has to recognize the target biomarker on a cell, but the corresponding signal from the reagent on cells lacking the biomarker has to be sufficiently small. QDs represent the most widely studied nanocrystals for target applications, particularly for polychromatic flow cytometry. They provide a dramatic increase in the number of parameters that can be measured simultaneously. In their 2006 *Nature Medicine* paper describing development of the 17-color flow cytometry assay, Chattopadhyay et al.²¹ discussed the complications of nonspecific binding with the QD reagents that they use to extend the color range of their assay. They found that nonspecific binding was largely overcome by coating the quantum dot shells with poly(ethylene glycol) (PEG), allowing them to overcome a crucial hurdle in the development of these reagents for immunophenotyping. Although one imagines that these commercial samples have been optimized to minimize nonspecific adsorption, reports

continue to appear in the literature in which nonspecific adsorption of QDs is a problem.^{22,23}

A recent paper¹⁹ on the use of a solvent exchange protocol to coat hydrophobic NPs with a PEG-containing phospholipid provides an interesting perspective on these problems. The authors used 1,2-distearoylphosphatidylethanolamine–methylpoly(ethylene glycol) with a PEG chain of $M = 2000$ (DSPE-mPEG) to coat two sizes ($d = 6.5$ and 17 nm) of iron oxide NPs (IONPs) as well as two samples of CdSe/ZnS QDs. The IONPs were synthesized with a surface coating of oleic acid, and the CdSe/ZnS QDs had a surface coating of trioctylphosphine oxide (TOPO). By mixing the DSPE-mPEG with corresponding PEG analogues containing a terminal amino group, a terminal $-\text{COOH}$ group, or a terminal maleimide, the authors were able to control the surface coverage of the IONPs with PEG ligands and the density of reactive functionality per NP. In addition, the authors were able to conjugate the 17 nm IONPs with anti-mouse IgGs through thiol maleimide chemistry and also to attach a goat anti-human folate receptor-1 Ab to these NPs. ELISA experiments with the former and *in vitro* experiments with the latter demonstrated high target recognition efficiency and low nonspecific binding. While these results are impressive and hold promise for the future of this coating protocol, the authors comment in the Supporting Information that when they applied this approach to QDs, the coating efficiency varied significantly among different batches of QDs that they purchased. In the current state of the art, it is clear that we have much to learn about how to optimize the surface coatings for different types of NPs and that the approach to finding the optimal surface coating may vary with the nature of the core of the nanoparticle.

While there have been important advances in the past several years in the synthesis of lanthanide nanoparticles,^{24–26} control over surface chemistry is less well advanced than for QDs or iron oxide NPs. Several strategies have been examined with good success to provide colloidal stability in aqueous media in the presence of phosphate buffer or serum proteins. These include flash nanoprecipitation,²⁷ ligand exchange with PEG bidentate²⁸ or tetradeinate phosphonates,²⁹ and encapsulation with amphiphilic polymers.³⁰ These technologies have not yet advanced to the point where meaningful mass cytometry experiments have been carried out with lanthanide NPs labeled with Abs.

Our goal in this paper is to assess the enhancement in sensitivity above background that nanoparticle reagents can provide for detection of biomarkers by mass cytometry. We want to ask the question, can one detect as few as 100 protein molecules per cell? In order to sidestep many of the problems of reagents that have to function in the complex environment of cell suspensions, we have chosen to create “model cells” consisting of microgels of uniform size. These cross-linked carboxylated microgels consist of a copolymer of *N*-isopropylacrylamide (NIPAm), *N*-vinylcaprolactam (VCL), and 27 mol % methacrylic acid (MAA). We employ streptavidin (SAv) as a model biomarker. The choice of SAv as a model biomarker enables us to use biotinylated reagents to detect the SAv entities on the model “cell” surface. In this way, we can compare the mass cytometry signal of metal-chelating polymers with a biotin end group and ca. 50 metal ions per polymer as a mass cytometry reagent with biotinylated NaHoF_4 NPs with a core diameter $d = 12.9$ nm, containing ca. 15 000 Ho atoms per NP.

In mass cytometry experiments with cell suspensions, the cells are fixed, permeabilized, and then stained with an iridium intercalator.³¹ Each cell entering the plasma creates an ion cloud generating signals for ¹⁹¹Ir and ¹⁹³Ir, which the instrument recognizes as the signature of a cell event. For our model cells, the microgels (MGs) are loaded with ca. 10^7 TmF₃/MG. In analogy with experiments on cell suspensions, the mass cytometer recognizes a strong ¹⁶⁹Tm signal as the signature of a “cell” event.

These experiments are enabled by a lucky happenstance. While it is straightforward to conjugate proteins such as SAv to the surface of microgels using typical peptide coupling agents, this approach leads to covalent attachment of ca. 10^4 SAv/MG. It is difficult to attach only small numbers of proteins, on the order of 100–500 SAv, to the microgels. When we reacted the microgels with biotin, to be used in a sandwich assay, the reaction could be carried out to only low conversion. At higher conversion, the microgels precipitated. In this way, we obtained three samples of microgels containing small but different numbers of biotins per microgel. These are the samples that permit us to examine whether we can detect as few as 100 SAvs per microgel.

RESULTS AND DISCUSSION

The idea of using microgels as model cells is not new. The basic idea is to design a microgel that mimics one or more properties of a cell while avoiding the complications of working with intact cells. In one example, artificial biotinylated alginate microgels with cell-like surface chemistry were studied to model cell flow behavior and adhesion properties when they were passing through avidin-modified constrictions.³² In another study, extremely deformable triethylene glycol acrylate/2-carboxylethyl acrylate copolymer microgels exhibited cell mimicking properties of passive hemoglobin diffusion throughout the particles.³³ Recently, the Shea group³⁴ reported synthetic polymer hydrogels (50–65 nm in diameter) that have the remarkable ability to recognize the Fc fragment of IgGs and bind to them with high affinity.

The experiments described here employ microgels (MGs) synthesized by the precipitation copolymerization of NIPAm, VCL, MAA, and the cross-linker methylenebisacrylamide in a mole ratio of 56:14:27:3 identical to the sample V27 reported in ref 35. The $-COOH$ groups, largely localized in the core of the MG,^{36,37} were neutralized with 1 equiv of NaOH, ion exchanged with Tm³⁺, and then TmF₃ was precipitated in the core of the micelle by the addition of NaF. We refer to these particles as MG(Tm). They were characterized for particle size by DLS ($d_h = 700$ nm, in PBS buffer at pH 7.4) and transmission electron microscopy (TEM, $d_{TEM} = 350 \pm 20$ nm, Figure 1A) and by mass cytometry to determine a mean Tm content (1.1×10^7 Tm atoms per microgel). This protocol is identical to that described for the preparation of EuF₃-containing MGs of sample V27 described in ref 35, where we demonstrated that the Ln ion content of the MGs saturated at 1 Ln³⁺ ion for every 3 $-COOH$ groups. From these results, we infer that our sample contains an average of $3.3 \times 10^7 -COOH$ groups per microgel. We used this value to calculate microgel concentrations in units of microgels/mL.

Attachment of SAv to the Microgels. SAv was chosen as the model biomarker to allow us to take advantage of the strong biotin–streptavidin interaction ($K_d \sim 10^{-14}$ M)³⁸ in our probe design. We used two approaches to attach SAv to the microgels. Details are provided in the Supporting Information. In the first

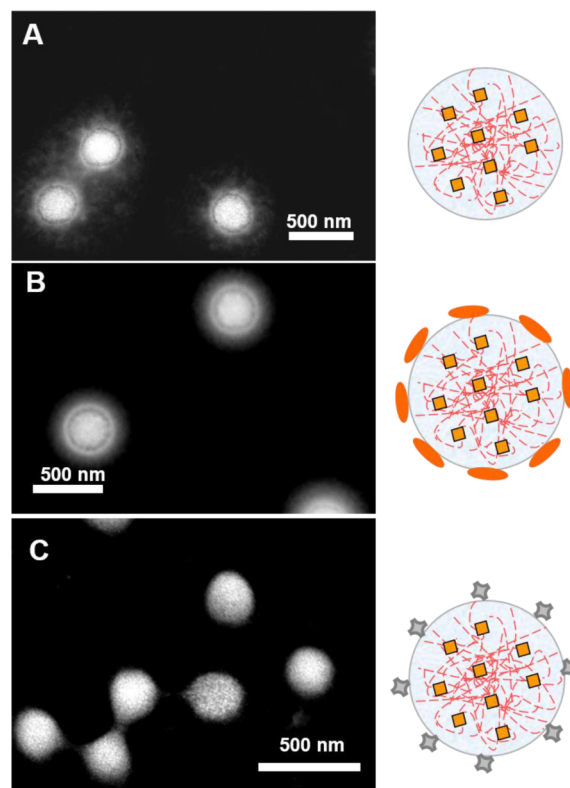


Figure 1. TEM images for the functional microgels described in the text: (A) MG(Tm); (B) BSA-MG(Tm); (C) SAv-MG(Tm). The microgels are characterized by $d_{MG(TM)} = 350 \pm 20$ nm, $d_{BSA-MG(TM)} = 330 \pm 20$ nm, and $d_{SAv-MG(TM)} = 230 \pm 20$ nm. Scale bars are 500 nm.

approach, we activated the carboxylic acids with 4-(4,6-dimethoxy-1,3,5-triazin-2-yl)-4-methylmorpholinium chloride (DMTMM) to attach SAv covalently to the microgels, presumably by coupling to lysine amino groups. This led to a high SAv content per microgel. We refer to these samples as SAv-MG(Tm). As a control, we used similar chemistry to attach BSA to these microgels (BSA-MG(Tm)). These reactions were quenched by adding excess 6-aminocaproic acid (6-ACA) to block unreacted activated carboxylic acid groups.

In the transmission electron microscopy (TEM) image in Figure 1A, the MG(Tm) microgels show a dense core associated with the presence of TmF₃ NPs surrounded by a diffuse corona. The BSA-MG(Tm) microgels (Figure 1B) and SAv-MG(Tm) microgels (Figure 1C) show more compact structures, which are rather different in appearance, with the SAv-MG(Tm) structures appearing to be more dense and more compact than either the BSA-MG(Tm) or MG(Tm) microgels. Dynamic light scattering (DLS) measurements indicated a small contraction in the hydrodynamic diameters of the modified microgels compared to MG(Tm) [$d_h(BSA-MG(TM)) = 640$ nm; $d_h(SAv-MG(TM)) = 640$ nm; $d_h(MG(TM)) = 700$ nm]. These values imply a more significant contraction of the microgel host, since attachment of protein molecules to the surface should add to the diameter of the overall objects. In the cartoons accompanying the TEM images in Figure 1, we attempt to depict the shape of the protein molecules, recognizing that the drawing is not to scale. The BSA protein is a prolate ellipsoid, 14×4 nm.³⁹ SAv is approximately spherical ($d \approx 7$ nm).⁴⁰ We depict it as a square to emphasize that it can bind four biotin moieties.

In a second approach, we attached biotin covalently to the microgel using DMTMM as a coupling agent and (+)-biotinyl-3,6-dioxaoctanediamine (Bi-NH_2) as the biotin source. The attachment yields were low, with only 5–10% of the added Bi-NH_2 consumed in the reaction. Attempts to attach larger amounts of biotin led to precipitation of the microgels. Three samples [Bi-MG(Tm)-1, -2, and -3; see Table S1] were obtained with different levels of biotin attached. To attach SAv to these microgels, they were first treated with a solution of BSA (1 wt % in PBS buffer) to saturate sites of nonspecific protein adsorption, followed, after washing, by a solution of SAv (1 wt % in PBS buffer). In these three SAv-Bi-MG(Tm) samples, we anticipate that the SAv molecules are confined to the MG surface. While we estimate that the microgels contain on average ca. 10^5 biotin moieties, many of these may be buried in the interior of the microgel.

Reagents for Biotin–Streptavidin Coupling Bioassays.

In current mass cytometry immunoassays, cell suspensions are treated with a cocktail of antibodies, each covalently labeled with metal chelating polymers (MCPs). In our model system, SAv serves as the model biomarker; thus, we need an MCP with biotin end-functionality as the recognition element. As an MCP, we employ a biotin-end-capped polyaspartamide synthesized as described previously,⁴¹ with diethylenetriamine-pentaacetic acid (DTPA) groups attached to each of its 50 pendant groups. Details are provided in the Supporting Information. This probe, labeled with ca. 50 Tb^{3+} ions/polymer, is denoted Bi-PAsp(Tb)₅₀. In Figure S8, we show a TEM image that confirms the ability of this polymer to bind to SAv-MG(Tm) microgels.

As a higher sensitivity probe, we introduce biotinylated NaHoF_4 nanoparticles (NPs). The NPs themselves, with oleic acid as surface ligands, were synthesized as described by Qian and Zhang,²⁵ subjected to ozonolysis $-78\text{ }^\circ\text{C}$ in hexane followed by oxidation with H_2O_2 as described by Yan and co-workers,⁴² to obtain an aqueous dispersion of NPs. These were then biotinylated with Bi-NH_2 using DMTMM as a coupling agent. Details are provided in the Supporting Information, and a dark field TEM image of these biotinylated NPs (Bi-NaHoF_4) is presented in Figure 2A. By TEM, these NPs have a mean diameter of 12.9 nm and contain ca. 15 000 Ho atoms per NP.

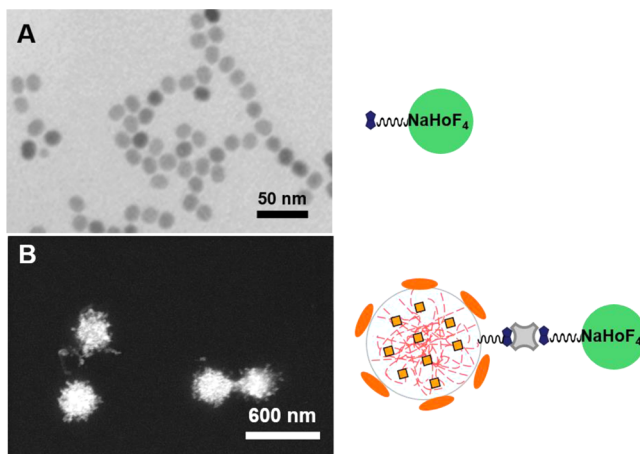


Figure 2. TEM images: (A) bright field image of biotinylated NaHoF_4 nanoparticles (Bi-NaHoF_4); (B) dark field TEM image of four biotinylated microgels treated successively with BSA, then SAv, and finally with Bi-NaHoF_4 . The drawings at the right are not to scale.

The size of the NPs in solution is important because its steric hindrance determines how many NPs can bind to each SAv on the microgel surface. By DLS at 90° (Figure S3), we determined a hydrodynamic radius in water of 14 nm.

As a test of binding, we used TEM to examine one sample [Bi-MG(Tm)-1] of biotinylated microgel. This microgel sample treated successively with BSA, then SAv, and finally with Bi-NaHoF_4 (i.e., SAv-Bi-MG(Tm)-Bi-NaHoF₄) shows a rough surface morphology (due to the presence of Bi-NaHoF_4 NPs) with an average TEM diameter of 350 nm (Figure 2B). The EDX line scan of the two microgels in Figure 3 shows the coexistence of Tm from the microgel and Ho from the Bi-NaHoF_4 NP probe, confirming the formation of NP-biotin-SAv-biotin complexes on the microgels.

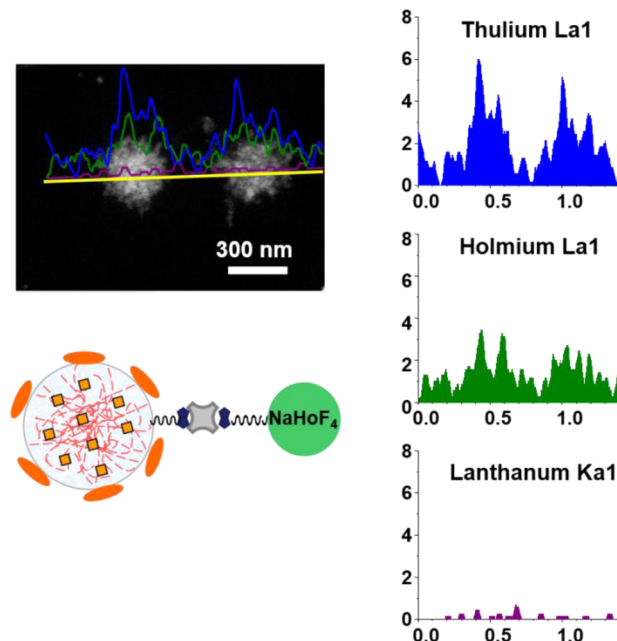
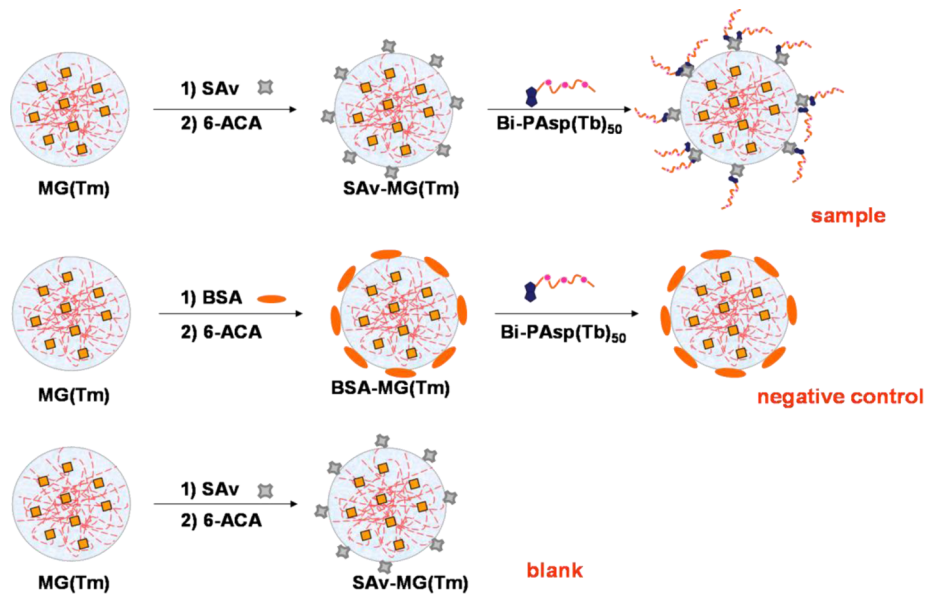


Figure 3. EDX linear scan through two biotinylated microgel particles, which were subjected to a streptavidin–biotinylated- NaHoF_4 –NP (biotin-SAv-biotin) sandwich assembly.

Biotin–Streptavidin Coupling Bioassays. The remainder of the paper examines the sensitivity of the reagents described above for detecting and quantifying the number of SAv, as a model biomarker, per microgel, as a model cell. The design of biotin–streptavidin coupling bioassays for the MCP reagent is shown in Scheme 1. We first incubated a sample of SAv-MG(Tm) microgels (covalently bound streptavidin) for 30 min with different amounts of Bi-PAsp(Tb)₅₀. Excess MCP was removed from the assembly by centrifugation and resuspension. As a negative control, we incubated samples of the BSA-coated microgel (BSA-MG(Tm)) with same amounts of Bi-PAsp(Tb)₅₀. Since there is no specific interaction between BSA and biotin, any Tb signal detected from this sample would be due to nonspecific interaction between the Bi-PAsp(Tb)₅₀ and the microgel. As a background blank, we examined the SAv-MG(Tm) without treatment with the biotinylated MCP.

Samples of SAv-MG(Tm) in PBS buffer were treated with increasing amounts of Bi-PAsp(Tb)₅₀. The mass cytometry data for this titration, presented in Figure 4, show both isotopic Tb–Tm dot–dot plots for the distribution of ^{159}Tb and ^{169}Tm signals (top row) and histograms of their relative abundance as

Scheme 1. Biotin–Streptavidin Coupling Bioassays^a

^aActivation of $-COOH$ groups on MG(Tm) with DMTMM and subsequent reaction with SAv or BSA was followed by 6-ACA to quench activated $-COOH$ groups. The modified microgels were then treated with Bi-PAsp(Tb)₅₀ and analyzed by mass cytometry.

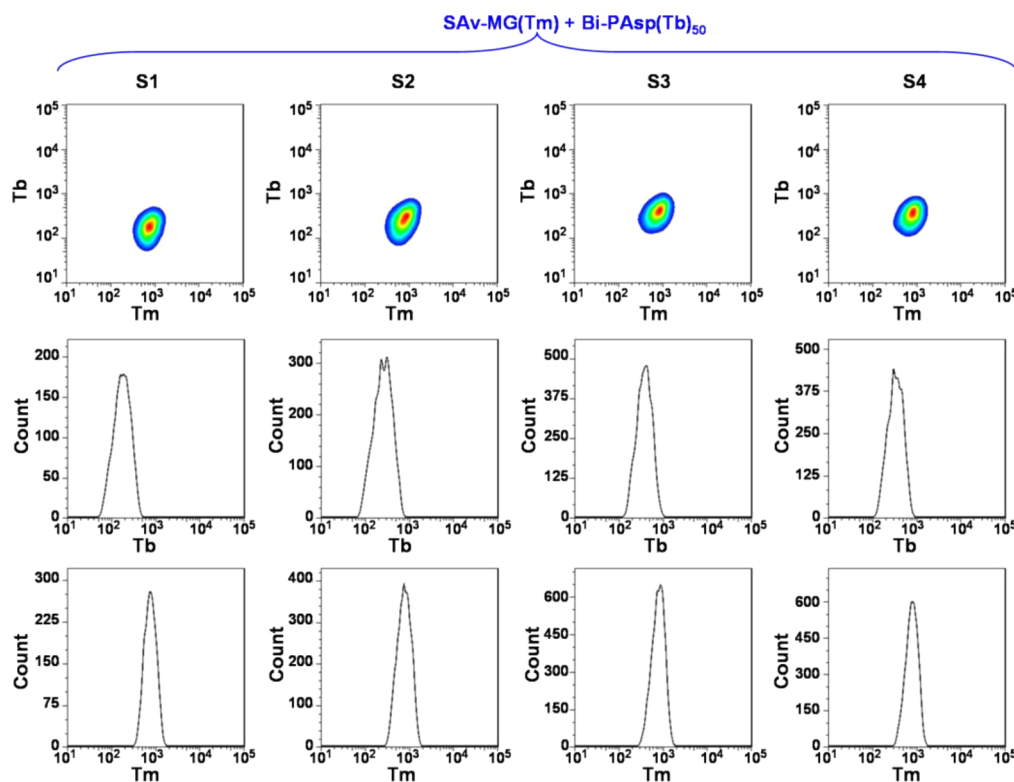


Figure 4. Isotopic Tb–Tm dot–dot plots (upper panel), histograms of Tb content distribution (middle panel), and histograms of Tm content distribution (lower panel) from the biotin–SAv coupling assays for SAv-MG(Tm) with Bi-PAsp(Tb)₅₀. In these experiments, SAv was covalently linked to the microgels. SAv-MG(Tm) (100 μ L, containing ca. 2.5×10^9 microgels in total) was incubated with different amounts of Bi-PAsp(Tb)₅₀ solution (3.3 μ mol/L: S1, 20 μ L; S2, 40 μ L; S3 60 μ L; S4 80 μ L). Data collection was gated to exclude “cell” debris and “cell” aggregates. At least 10 000 microgels were analyzed per sample.

characterized by the isotope intensities. For these SAv-MG(Tm)-Bi-PAsp(Tb)₅₀ assemblies, the signals for both ¹⁵⁹Tb and ¹⁶⁹Tm were strong, with a Pearson correlation (r) between the Tb and Tm signal intensities in the range of 0.70–0.90, a strong positive linear correlation.

As a control, we incubated samples of BSA-MG(Tm) with the same amounts of Bi-PAsp(Tb)₅₀. These data are presented in Figure 5, where the top row displays isotopic Tb–Tm dot–dot plots for the distribution of ¹⁵⁹Tb and ¹⁶⁹Tm signals. The second and third rows are histograms of their relative

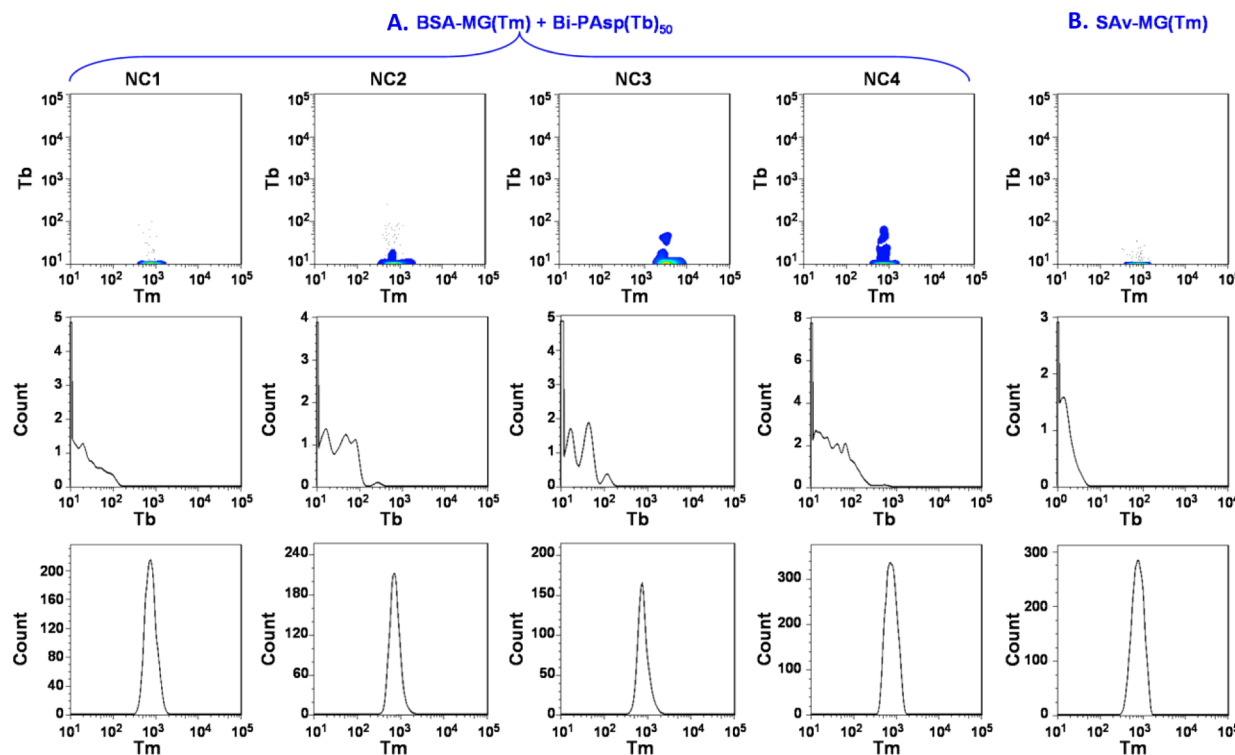


Figure 5. Isotopic Tb–Tm dot–dot plots (upper panel), histograms of Tb content distribution (middle panel), and histograms of Tm content distribution (lower panel) from the negative control and blank experiments related to those described in Figure 4. Part A: negative control (NC) experiments in which microgels covalently labeled with BSA (BSA-MG(Tm) 100 μ L, containing ca. 2.5×10^9 microgels in total) was incubated with different amounts of Bi-PAsp(Tb)₅₀ solution (3.3 μ mol/L: NC1, 20 μ L; NC2, 40 μ L; NC3, 60 μ L; NC4, 80 μ L). Part B: SAv-MG(Tm) microgel solution. Data collection was gated to exclude “cell” debris and “cell” aggregates. At least 10 000 microgels were analyzed per sample.

abundance as characterized by the isotope intensities. While the ¹⁶⁹Tm signals were strong, the Tb signals were weak, with $r = 0.15\text{--}0.20$, indicating that the Tb signals we detect were not strongly associated with the Tm signals of the microgels. As a blank, we examined SAv-MG(Tm) itself in the absence of any intentionally added source of Tb. Again, the Tm signal was strong, but the Tb signal was very weak with $r < 0.02$. Since no specific interaction is expected between the polymer and the BSA-coated microgel, the differences between the Tb signals for the control and blank samples are a measure of nonspecific interaction of the MCP with the BSA-coated microgel.

Histograms describing the numbers of Tm and Tb atoms per microgel calculated from these experiments are presented in Figure 6. Titration of the SAv-MG(Tm) solutions with increasing amounts of Bi-PAsp(Tb)₅₀ led to a saturation level of 4×10^6 Tb atoms per microgel. In the negative control experiments with BSA-MG(Tm), the Tb numbers were much smaller, corresponding to a nonspecific binding signal of 4–6%. For comparison, the SAv-MG(Tm) microgels that serve as a blank show a background signal corresponding to ca. 3×10^4 Tb atoms per microgel (i.e., ca. 1% of background contamination). Figure 6B (lower panel) shows that all of the samples exhibited a similar Tm intensity, corresponding to 1.1×10^7 Tm atoms per cell, with a typical CV of ca. 30%.

To estimate the number of SAv biomarkers per cell, we have to make some assumptions about the interaction between the SAVs on the microgel surface and the biotinylated MCP. Each Bi-PAsp(Tb)₅₀ carries an average of 50 Tb ions. Streptavidin has four binding sites. If we assume that each SAv binds to four biotin-end-capped polymers, then each SAv would carry 200 Tb ions at saturation. Since at saturation, the microgels contain

ca. 4.0×10^6 Tb atoms per microgel, then on average each microgel carries 20 000 SAv biomarkers. This is a reasonable number and may be an underestimate due to the inaccessibility of some biotin binding sites. A geometric model shows that a sphere with a radius of 320 nm (the size of the SAv-coated microgels) can accommodate a layer of 3.0×10^4 close-packed spheres with $d = 7$ nm (the size of a SAv molecule). To the extent that the assumptions made above are correct, our streptavidin-coated microgels have a surface packing density of 67%.

Biotin–SAv–Biotin Sandwich Assays. A second set of assays employed biotinylated microgels. As described above, we were limited in the amount of biotin that we could attach covalently to the microgels. As a consequence, the number of SAv biomarkers per microgel was smaller than in the examples described above. With the SAv-Bi-MG(Tm) samples prepared from the three Bi-MG(Tm) microgels described in Table S1, we carried out binding assays with two types of biotin containing reagents: Bi-PAsp(Tb)₅₀ and Bi-NaHoF₄. The experimental design is summarized in Scheme 2.

The first set of binding experiments were carried out with Bi-PAsp(Tb)₅₀ (for details, see Supporting Information and Figure S9), where we treated aliquots of the SAv-coated microgels (100 μ L, ca. 2.5×10^9 microgels, 6.2×10^5 biotin/microgel), with increasing amounts of Bi-PAsp(Tb)₅₀ solution (0.33 μ mol/L: 10 μ L; 20 μ L; 40 μ L; 80 μ L). While the mass cytometry measurements showed strong Tm signals for the microgels, all samples showed very weak Tb signals, between 1 and 10 counts/microgel. With increasing amounts of added Bi-PAsp(Tb)₅₀ we obtained stronger Tb signals from both SAv-Bi-MG(Tm) and BSA/MG(Tm) microgels. However, the

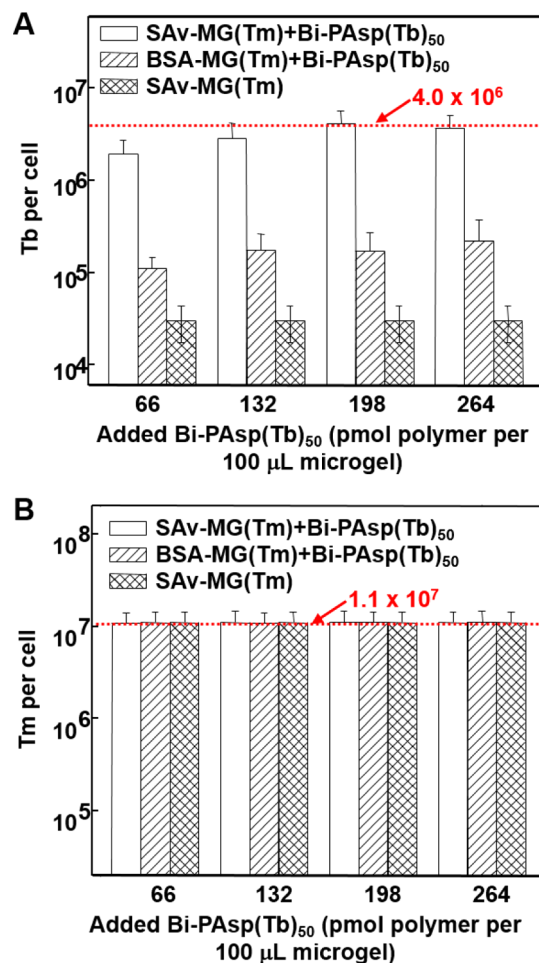


Figure 6. Tb and Tm content per microgel determined by mass cytometry from biotin-SAv coupling assays. Numbers of Tb and Tm atoms per cell were calculated using the mass cytometry transmission coefficient for Tb ions of 9.88×10^{-5} and for Tm ions of 7.30×10^{-5} . For SAv-MG(Tm) and BSA-MG(Tm) samples, the amounts of Bi-PAsp(Tb)₅₀ employed are indicated on the x-axis. The SAv-MG(Tm) samples not treated with metal chelating polymer are indicated by the cross-hatched bars in the histograms. The data are replotted from Figures 4 and 5. (A) After treating the SAv-MG(Tm) solutions (containing ca. 2.5×10^9 microgels) with 66, 132, 198, and 264 pmol of Bi-PAsp(Tb)₅₀, we obtained $(1.9 \pm 0.8) \times 10^6$, $(2.8 \pm 1.3) \times 10^6$, $(4.1 \pm 1.5) \times 10^6$, and $(3.6 \pm 1.4) \times 10^6$ Tb atoms per microgel, respectively. The red line indicates the saturation level for SAv-MG(Tm) + Bi-PAsp(Tb)₅₀ of 4.0×10^6 Tb atoms per cell microgel. In the negative control experiments with BSA-MG(Tm), the Tb correspond to $(1.1 \pm 0.4) \times 10^5$, $(1.7 \pm 0.8) \times 10^5$, $(1.7 \pm 1.0) \times 10^5$, and $(2.2 \pm 1.5) \times 10^5$ Tb atoms per microgel. SAv-MG(Tm) microgels (the blank) show a background signal corresponding to $(3.0 \pm 1.3) \times 10^4$ Tb atoms per microgel. (B) The red line indicates a mean value of 1.1×10^7 Tm atoms per microgel for all samples. The error bars indicate the cell-by-cell coefficient of variation of lanthanide ion content ($CV_{Ln} = \text{ca. } 30\%$ for all samples) determined from gated mass cytometry data.

difference in Tb intensity from the Bi-Asp(Tb)₅₀ treated SAv-Bi-MG(Tm) samples and BSA/MG(Tm) samples was very small, with a maximum signal-to-noise ratio of 1.2. Thus, we conclude that the number of SAvs on the surface of the biotinylated microgels was too small to be detected by mass cytometry with the current generation instrument using a metal chelating polymer as a reagent.

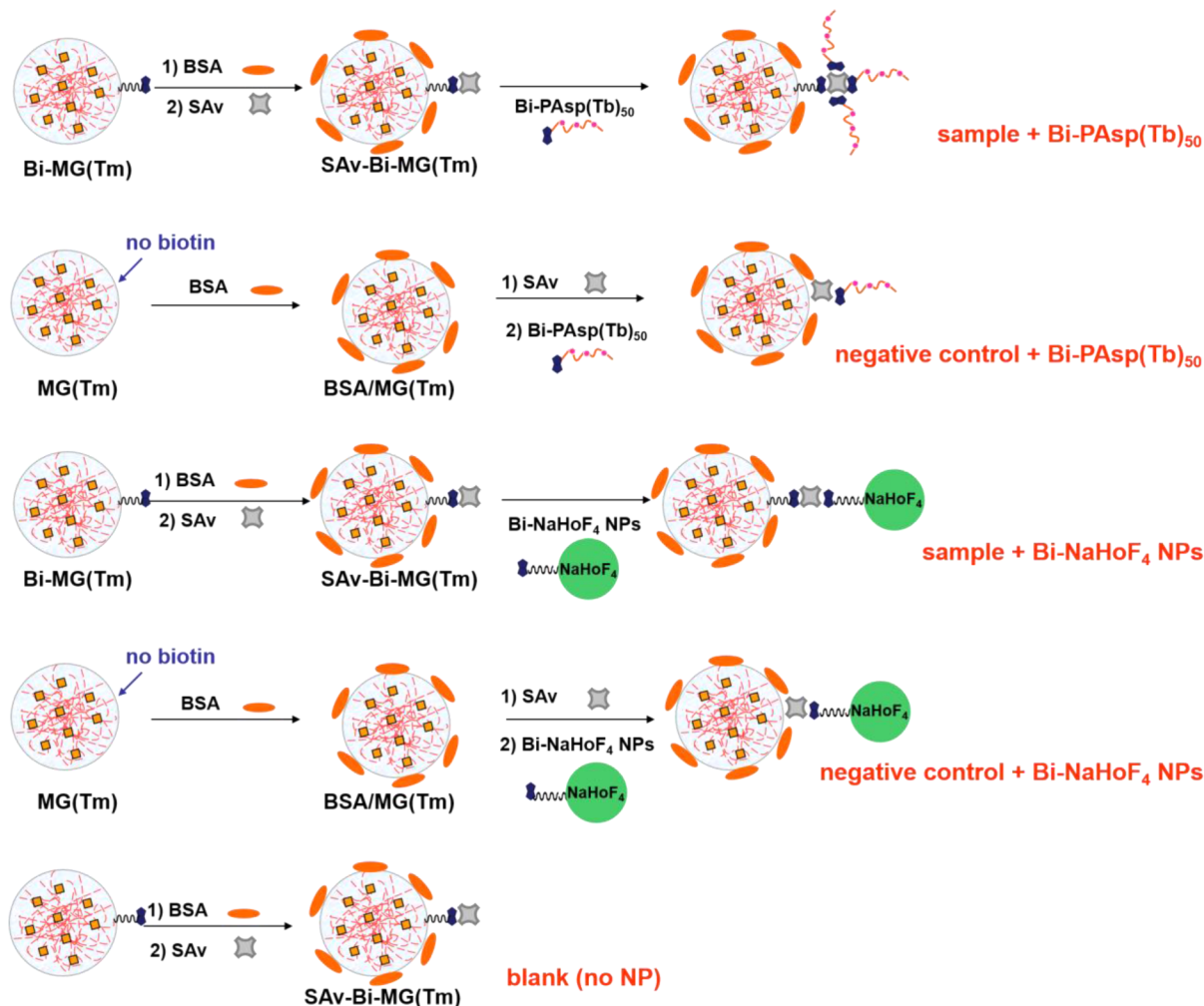
Then we tested the sensitivity of the Bi-NaHoF₄ NPs. Each of the three SAv-Bi-MG(Tm) microgel samples (100 μL , each containing ca. 2.5×10^9 microgels) was incubated with excess NPs (0.05 mg, 0.015 μmol). Excess NPs were removed from the sandwich assembly via three cycles of centrifugation and resuspension of the microgels, followed by analysis by mass cytometry. The data for these experiments and the corresponding control and blank measurements are presented in Figure 7. The top row in Figure 7A displays isotopic Ho–Tm dot-dot plots for the distribution of ¹⁶⁵Ho and ¹⁶⁹Tm signals for the SAv-Bi-MG(Tm) samples. The units on the x- and y-axes of these plots are the measured intensities for the respective isotopes. In the second and the third rows, the data are replotted as histograms showing the relative abundance of microgels characterized by the isotope intensities displayed on the x-axes. For these SAv-Bi-MG(Tm)-Bi-NaHoF₄ assemblies, the signals for both ¹⁶⁵Ho and ¹⁶⁹Tm are strong. The Pearson correlation between the Tm and Ho signal intensities was ca. 0.60 from the three batches of samples. This value indicates that the Ho signals detected are strongly associated with the Tm signals of the microgels.

In parallel, we treated BSA-passivated biotin-free microgels (BSA/MG(Tm)) first with SAv and, after washing, with Bi-NaHoF₄ NPs. The corresponding mass cytometry data are shown in Figure 7B. The Tm signal is strong; however, the Ho signal is much weaker. The Pearson correlation between Tm and Ho signal intensities was $r = 0.20$, which indicates a weak linear correlation between the two ions in this negative control sample. As a blank, we examined the SAv-Bi-MG(Tm) itself in the absence of any intentionally added source of Ho. These data are shown in the three plots in Figure 7C. While the Tm signal was strong, the Ho signal was weak, with a very little correlation ($r < 0.01$) found between Tm and Ho signals.

The calculated numbers of metal ions per microgel are plotted as a bar graph in Figure 8. For the SAv-Bi-MG(Tm)-Bi-NaHoF₄ complexes, we obtained $(1.6 \pm 0.6) \times 10^6$ Ho atoms per microgel for SAv-Bi-MG(Tm)-1, $(3.1 \pm 0.7) \times 10^6$ Ho atoms per microgel from SAv-Bi-MG(Tm)-2, and $(6.0 \pm 0.9) \times 10^6$ Ho atoms per microgel from SAv-Bi-MG(Tm)-3. In contrast, for the negative control (BSA/MG(Tm)), we obtained $(2.9 \pm 1.2) \times 10^5$ Ho atoms per cell. This signal level corresponds to a nonspecific binding signal of 5–18%. The SAv-Bi-MG(Tm) microgels that serve as a blank and show a background signal corresponding to $(2.4 \pm 4.9) \times 10^4$ Ho atoms per microgel (ca. 1% background contamination). Figure 8B (lower panel) shows that all the microgel hybrids exhibited a similar Tm intensity, 1.1×10^7 Tm atoms per microgel, with a typical CV of ca. 30%.

Dividing the Ho number per cell by the Ho number per nanoparticle (15 000) yields the average number of nanoparticles per cell. From the three different SAv-Bi-MG(Tm)-Bi-NaHoF₄ complexes, we obtained 107 ± 40 , 205 ± 47 , and 400 ± 60 NaHoF₄ nanoparticles per cell. For the negative control (BSA/MG(Tm)), we found 19 ± 8 nanoparticles bound nonspecifically per cell. From the blank, we detected a background contamination level equivalent to 2 ± 3 nanoparticles per microgel.

With at least one of the SAv binding sites already attached to the cell surface, a maximum of three biotin binding sites are available for additional binding with nanoparticles. Since, however, we have no direct calibration of the number of NPs that can bind to each accessible SAv, it is problematic to convert numbers of NPs bound per microgel to absolute

Scheme 2. Biotin–Streptavidin–Biotin Sandwich Assays^a

^aBiotinylated and biotin-free MG samples were first treated with BSA and then SAv. After washing they were treated with Bi-PAsp(Tb)₅₀ or Bi-NaHoF₄ NPs and analyzed by mass cytometry.

numbers of biomarkers. In the Supporting Information, we develop a geometric argument that suggests that if the microgel and the NPs were hard spheres with radii equal to their hydrodynamic radius, then for NPs with radii in the range $10.1 \text{ nm} < r_{NP} \leq 13.0 \text{ nm}$, the maximum packing number would be 2 per SAv, and for larger NPs, the maximum packing number is 1 per SAv. This argument has two limitations. First, surface irregularities in the microgel may make some SAvs inaccessible to the NPs. Second, the NaHoF₄ NPs (with $r_h = 14 \text{ nm}$, see Figure S3) may deform in a way that allows more than one NP to bind to a SAv. Therefore, the most important conclusion of this work is that we can detect very small numbers of NPs per microgel, as few as 100–500 nanoparticles bound to biomarkers per microgel, and the detection limit is determined more by nonspecific adsorption of NPs to the microgels than by the sensitivity of the mass cytometer measurement.

SUMMARY AND CONCLUSIONS

In this paper, we examined the sensitivity of different reagents for detecting and quantifying by mass cytometry the number of SAv, as a model biomarker, per microgel, as a model cell. In our system, the microgel was labeled with TmF₃, so that the detection of ¹⁶⁹Tm ions served as the signature of a “cell” event.

The streptavidin biomarkers were then detected with biotinylated probes, from which we were able to quantify the number of probes bound per model cell.

We used two approaches to attach SAv biomarkers to the microgel. Carboxyl activation chemistry to attach SAv covalently to the microgels led to a high SAv content. In contrast, covalent attachment of biotin, passivation with BSA, and subsequent treatment with SAv led to low SAv contents per microgel. Two types of biotinylated probes were used: a biotinylated MCP (Bi-PAsp(Tb)₅₀, containing on average 50 Tb³⁺ ions atoms per probe) and biotinylated NaHoF₄ NPs (Bi-NaHoF₄, containing ca. 15 000 Ho atoms per probe). For microgels carrying high abundance of SAv biomarkers, the interaction of the metal-chelating polymer Bi-PAsp(Tb)₅₀ with the SAv-coated microgels was much stronger than the interaction with BSA-coated microgels, used as a negative control to account for nonspecific absorption. From this approach a biomarker level at ca. 10⁴ per cell was detected by mass cytometry.

For microgels carrying low copy numbers of streptavidin biomarkers, the Bi-PAsp(Tb)₅₀ reagent gave a very low signal, not significantly different from that with the BSA-coated microgel sample. With current instrumentation, this type of

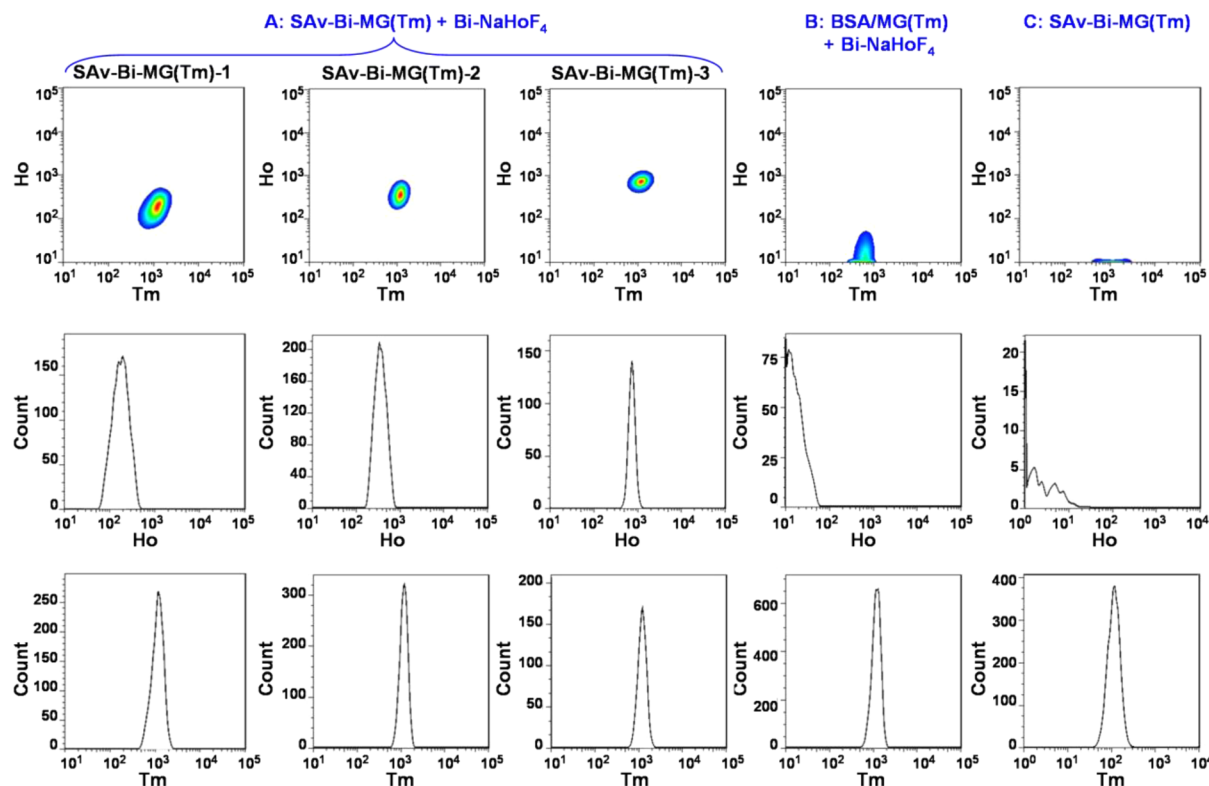


Figure 7. Isotopic Ho–Tm dot–dot plots (upper panel), histograms of Ho content distribution (middle panel), and histograms of Tm content distribution (lower panel) from biotin–SAv–biotin sandwich assays. Part A: SAv-Bi-MG(Tm) microgel solution in PBS buffer (100 μ L, containing ca. 2.5×10^9 microgels) were incubated with excess of Bi-NaHoF₄ NPs (0.015 μ mol in 10 μ L of DI water). Part B: BSA/MG(Tm) solution in PBS buffer (100 μ L, containing ca. 2.5×10^9 microgels) were incubated with SAv solution (500 nmol/L, 10 μ L, 0.005 nmol) and then with excess of Bi-NaHoF₄ NPs (0.015 μ mol in 10 μ L of DI water). Part C: SAv-Bi-MG(Tm) microgels containing ca. 2.5×10^9 microgels. Data collection was gated to exclude cell debris and cell aggregates. At least 10 000 cells were analyzed per sample.

MCP reagent does not generate sufficient signal to measure these low levels of biomarkers per cell.

In contrast, the biotinylated NaHoF₄ NPs (with 15 000 Ho atoms per NP) gave a mass cytometry signal about 2 orders of magnitude stronger, while maintaining a relatively low signal level from nonspecific absorption. In the sandwich assay described here, for the three SAv-Bi-MG(Tm) samples examined, we determined signal levels of ca. 400 ± 60 , 200 ± 50 , and 100 ± 40 NPs per microgel. While the background signal was very low, the sensitivity of the measurements was limited by nonspecific interaction of the NPs with the BSA-coated microgels, determined to be ca. 20 NPs per microgel. This proof of concept experiment demonstrates the enhanced sensitivity possible with NP reagents in cell-by-cell assays by mass cytometry.

Applying this knowledge to biological samples requires significant improvement in the surface coating of lanthanide nanoparticles, to optimize the type and number of surface functional groups for attachment to antibodies, to optimize purification of the NP-Ab conjugates, and to minimize nonspecific interaction with cells. This is an ongoing task in our laboratory and elsewhere.

EXPERIMENTAL SECTION

Materials. The poly(NIPAm/VCL/MAA) copolymer microgel sample employed here is the same sample as that denoted V27 in ref 35. The original sample at ca. 0.85 wt % solids was repurified by sedimentation–redisposition in deionized water, and its concentration in terms of total acid content was determined by titration. This sample was loaded with TmF₃ (denoted MG(Tm)) following the protocol

described in ref 35 for EuF₃-loaded microgels. After ion exchange or chemical modification, all microgel samples were purified by three cycles of sedimentation by centrifugation (5000 rpm, 40 min, 23 °C) and redisposition in DI water and finally redisposed in PBS buffer and stored at 4 °C prior to use.

The details of the modification of the microgels by covalent attachment of SAv, BSA, or biotin are described in the Supporting Information.

The biotin end-capped metal chelating polymer probe (Bi-PAsp(Tb)₅₀) labeled with Tb³⁺ ions was synthesized following a protocol that we described previously.⁴¹ Details are provided in the Supporting Information. The synthesis and characterization of biotinylated NaHoF₄ nanoparticles are also described in the Supporting Information.

Streptavidin–Biotin Coupling Assays Employing Bi-PAsp(Tb)₅₀. Samples. Four aliquots of SAv-MG(Tm) solution (100 μ L, containing ca. 2.5×10^9 microgels) were incubated with different amounts of a Bi-PAsp(Tb)₅₀ solution (3.3 μ mol/L: 20 μ L, 40 μ L, 60 μ L, 80 μ L) for 30 min at room temperature. Then the solutions were purified from excessive polymer by three cycles of centrifugation at 5000 rpm for 40 min at RT followed by redisposition in DI water (1 mL). The concentration of the microgel solution was adjusted to ca. 10^6 microgels per mL with DI water for analysis by mass cytometry.

Negative Control. Four aliquots of BSA-MG(Tm) solution (100 μ L, containing ca. 2.5×10^9 microgels) were incubated with different amounts of a Bi-PAsp(Tb)₅₀ solution (3.3 μ mol/L: NC1, 20 μ L; NC2, 40 μ L; NC3, 60 μ L; NC4, 80 μ L) and stirred at room temperature for 30 min. Then the solutions were purified as described above by three cycles of centrifugation–redisposition with DI water (1 mL) and then diluted to 10^6 microgels per mL with DI water for analysis by mass cytometry.

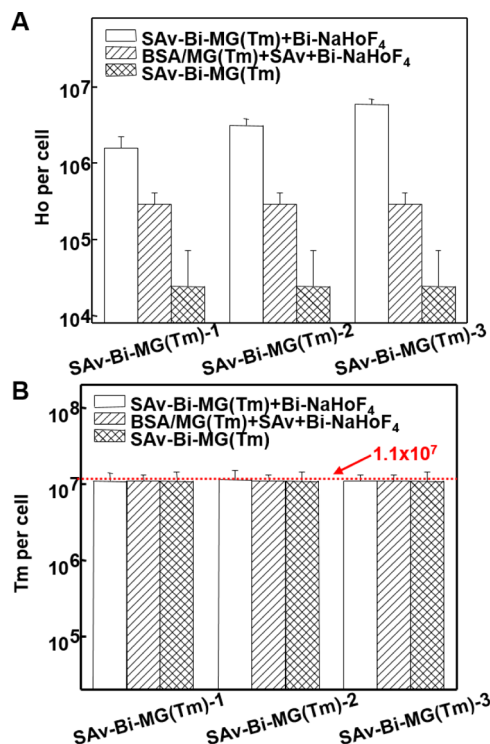


Figure 8. Ho and Tm intensities for cells from biotin–SAv–biotin sandwich assays. Numbers of Tm and Ho atoms per cell were calculated using mass cytometry transmission coefficients of 1.11×10^{-4} for Tm ions and 1.23×10^{-4} for Ho ions. (A) Ho content per microgel. The error bars indicate the cell-by-cell coefficient of variation of lanthanide ion content (CV_{Ln}) determined from gated mass cytometry data. (B) Tm content per microgel. The red line indicates a mean value of 1.1×10^7 Tm atoms per microgel for all samples, with a cell-to-cell CV of 30%.

Blank Control. A solution of streptavidin-coated microgel (SAv-MG(Tm), 100 μ L, containing ca. 2.5×10^9 microgels) was directly diluted to 10^6 microgels per mL with DI water for analysis by mass cytometry.

Biotin–Streptavidin–Biotin Sandwich Assays. Sample + Bi-PAsp(Tb)₅₀. Four aliquots of a solution of SAv-Bi-MG(Tm)-3 (100 μ L, containing ca. 2.5×10^9 microgels) were stirred for 30 min at room temperature with 6-aminocaproic acid (6-ACA, 0.03 μ mol in 3 μ L), then incubated with different amounts of a Bi-PAsp(Tb)₅₀ solution (0.33 μ mol/L: 10 μ L; 20 μ L, 40 μ L, 80 μ L), and stirred at room temperature for 30 min. Then the solutions were purified as described above by centrifugation–redisposition in DI water (1 mL) and then diluted to 10^6 microgels per mL with DI water for analysis by mass cytometry.

Sample + Bi-NaHoF₄. A solution of each of the three SAv-Bi-MG(Tm) microgels (100 μ L, containing ca. 2.5×10^9 microgels) was stirred with Bi-NaHoF₄ NPs solution in DI water (5 mg/mL, 10 μ L, 0.015 μ mol) for 30 min at room temperature. The solutions were purified by centrifugation–redisposition in 1 mL of DI water and then diluted to 10^6 microgels per mL with DI water for analysis by mass cytometry.

Negative Control + Bi-PAsp(Tb)₅₀. Four aliquots of a solution of microgels with a surface passivated with adsorbed BSA (BSA/MG(Tm), 100 μ L, containing ca. 2.5×10^9 microgels) were stirred with 6-aminocaproic acid (6-ACA, 0.03 μ mol in 3 μ L) for 30 min at room temperature and then incubated with SAv solution (500 nmol/L, 10 μ L, 0.005 nmol) for 30 min. After that, different amounts of a Bi-PAsp(Tb)₅₀ solution (0.33 μ mol/L: NC1, 10 μ L; NC2, 20 μ L; NC3, 40 μ L; NC4, 80 μ L) were added followed by stirring for 30 min at room temperature. Then the solutions were purified as described above by three cycles of centrifugation–redisposition in DI water (1

mL) and then diluted to 10^6 microgels per mL with DI water for analysis by mass cytometry.

Negative Control + Bi-NaHoF₄. A solution of SAv (500 nmol/L, 10 μ L, 0.005 nmol) was added to a solution of microgels with a surface passivated with adsorbed BSA (BSA/MG(Tm), 100 μ L, containing ca. 2.5×10^9 microgels) and stirred for 30 min. Then a solution of Bi-NaHoF₄ in DI water (5 mg/mL, 10 μ L, 0.015 μ mol) was added, and stirring was continued for 30 min at room temperature. The solution was purified by three sedimentation/redisposition cycles as described above to remove excess NaHoF₄ nanoparticles, which did not sediment under these conditions. In the final step, the microgels were redispersed in DI water (1 mL). Before analysis, the microgel solution was diluted with DI water to ca. 10^6 microgels per mL.

Blank Control. A solution of SAv-Bi-MG(Tm) (100 μ L, containing ca. 2.5×10^9 microgels) was diluted to ca. 10^6 microgels per mL with DI water before characterization.

Instrumentation. Mass Cytometry. Mass cytometry experiments were carried out using a model C2 instrument (CyTOF) from DVS Sciences (Markham, ON, Canada).³ Samples were examined at a rate of ca. 1000 microgels/s. Ion signals were collected by dual-counting, the combination of digital counting and analogue modes of ion detection, which allows a much wider range of ion signal (simultaneous detection of very small and very large signals). The data were collected in FCS 3.0 format and were processed by FlowJo software.

The average number of metal ions per microgel, N , can be calculated from the mean intensity values measured by the TOF detector, I , through the expression $N = I/T$, where T is the transmission coefficient and corresponds to the number of ions that reach the detector per number of ions injected. T values were determined on a daily basis using a standard solution that contained different lanthanide ions that cover the lanthanide series mass range (La, Tb, and Tm at 0.5 ppb w/w). Using the mass response (number of counts from the mass cytometry detector) to the known concentration of the ions, values of T were calculated for each ion in the standard solution.

ASSOCIATED CONTENT

S Supporting Information

Additional information including experimental details for synthesis and characterization of the microgels, the metal chelating polymer and the NaHoF₄ nanoparticles; pH and conductometric titration of microgels; mass cytometry screen captures from SAv-Bi-MG(Tm)/Bi-NaHoF₄ NPs sandwich bioassays; estimation of the number of Bi-NaHoF₄ NP per streptavidin on SAv-Bi-MG(Tm) microgels; quantification of biotinylation reaction by UV-vis spectrometry; hydrodynamic radius of microgel samples determined from multiangular dynamic light scattering; estimation of average mesh size of the microgels; estimation of the number of Ho atoms per Bi-NaHoF₄ NP, apparent zeta potential and electrophoretic mobility for microgel samples in SAv-biotin coupling assays; Tb–Tm dot-dot plots, Tb and Tm histograms, and graphs for Tb and Tm content per microgel determined by mass cytometry for Bi-SAv-Bi sandwich assays with Bi-PAsp(Tb)₅₀ as the detecting reagent; geometric analysis of NP binding to SAv on the surface of a microgel. This material is available free of charge via the Internet at <http://pubs.acs.org>.

AUTHOR INFORMATION

Corresponding Author

*Tel +1 416 978 6495; e-mail mwinnik@chem.utoronto.ca (M.A.W.).

Author Contributions

W.L. conducted the experiments. Y.H. prepared and characterized the NaHoF₄ nanoparticles. Y.L. prepared and

characterized the metal-chelating polymers, which were further characterized by L.T. and G.Z. P.C. contributed a review of background literature. A.I.A. conducted initial mass cytometry tests. J.Q. characterized the microgels by DLS. M.A.W. originated the research idea. V.B. and M.N. assisted with experimental design and data interpretation. W.L., M.N. and M.A.W. wrote the manuscript, and all authors have given approval to the final version of the manuscript.

Notes

The authors declare no competing financial interest, except for V.B., a Principal Scientist at DVS Sciences Inc.

ACKNOWLEDGMENTS

The authors thank NSERC Canada, DVS Sciences, and the Office of AIDS Research at the National Institutes of Health for their financial support and Dr. Olga Ornatsky for helpful discussions on the design of model assays.

REFERENCES

- (1) Atkinson, A. J.; Colburn, W. A.; DeGruttola, V. G.; Demets, D. L.; Downing, G. J.; Hoth, D. F.; Oates, J. A.; Peck, C. C.; Schooley, R. T.; Spilker, B. A.; Woodcock, J.; Zeger, S. L. Biomarkers and Surrogate Endpoints: Preferred Definitions and Conceptual Framework. *Clin. Pharmacol. Ther.* **2001**, *69*, 89–95.
- (2) Perfetto, S. P.; Chattopadhyay, P. K.; Roederer, M. Seventeen-Colour Flow Cytometry: Unravelling the Immune System. *Nat. Rev. Immunol.* **2004**, *4*, 648–655.
- (3) Bandura, D. R.; Baranov, V. I.; Ornatsky, O. I.; Antonov, A.; Kinach, R.; Lou, X.; Pavlov, S.; Vorobiev, S.; Dick, J. E.; Tanner, S. D. Mass Cytometry: Technique for Real Time Single Cell Multitarget Immunoassay Based on Inductively Coupled Plasma Time-of-Flight Mass Spectrometry. *Anal. Chem.* **2009**, *81*, 6813–6822.
- (4) Lou, X.; Zhang, G.; Herrera, I.; Kinach, R.; Ornatsky, O.; Baranov, V.; Nitz, M.; Winnik, M. A. Polymer-Based Elemental Tags for Sensitive Bioassays. *Angew. Chem., Int. Ed.* **2007**, *46*, 6111–6114.
- (5) Majonis, D.; Herrera, I.; Ornatsky, O.; Schulze, M.; Lou, X.; Soleimani, M.; Mark Nitz, M.; Winnik, M. A. Synthesis of a Functional Metal-Chelating Polymer and Steps toward Quantitative Mass Cytometry Bioassays. *Anal. Chem.* **2010**, *82* (21), 8961–8969.
- (6) Illy, N.; Majonis, D.; Herrera, I.; Ornatsky, O.; Winnik, M. A. Metal-Chelating Polymers by Anionic Ring-Opening Polymerization and Their Use in Quantitative Mass Cytometry. *Biomacromolecules* **2012**, *13* (8), 2359–2369.
- (7) Bendall, S. C.; Nolan, G. P.; Roederer, M.; Chattopadhyay, P. K. A Deep Profiler's Guide to Cytometry. *Trends Immunol.* **2012**, *33*, 323–332.
- (8) Bendall, S. C.; Simonds, E. F.; Qiu, P.; Amir, E. D.; Krutzik, P. O.; Finck, R.; Bruggner, R. V.; Melamed, R.; Trejo, A.; Ornatsky, O. I.; Balderas, R. S.; Plevritis, S. K.; Sachs, K.; Pe'er, D.; Tanner, S. D.; Nolan, G. P. Single-Cell Mass Cytometry of Differential Immune and Drug Responses across a Human Hematopoietic Continuum. *Science* **2011**, *332*, 687–696.
- (9) Newell, E. W.; Sigal, N.; Bendall, S. C.; Nolan, G. P.; Davis, M. M. Cytometry by Time-of-Flight Shows Combinatorial Cytokine Expression and Virus-Specific Cell Niches within a Continuum of CD8+ T Cell Phenotypes. *Immunity* **2012**, *36*, 142–152.
- (10) Newell, E. W.; Sigal, N.; Nair, N.; Kidd, B. A.; Greenberg, H. B.; Davis, M. M. *Nat. Biotechnol.* **2013**, *31* (7), 623–629.
- (11) Bodenmiller, B.; Zunder, E. R.; Finck, R.; Chen, T. J.; Savig, E. S.; Bruggner, R. V.; Simonds, E. F.; Bendall, S. C.; Sachs, K.; Krutzik, P. O.; Nolan, G. P. Multiplexed Mass Cytometry Profiling of Cellular States Perturbed by Small-Molecule Regulators. *Nat. Biotechnol.* **2012**, *30* (9), 858–867.
- (12) Kettman, J. R.; Coleclough, C.; Frey, J. R.; Lefkovits, I. Clonal Proteomics: One Gene – Family of Proteins. *Proteomics* **2002**, *2*, 624–631.
- (13) Newman, J.; Ghaemmaghami, S.; Ihmels, J.; Breslow, D.; Noble, M.; Derisi, J.; Weissman, J. Single-Cell Proteomic Analysis of *S. Cerevisiae* Reveals the Architecture of Biological Noise. *Nature* **2006**, *441*, 840–846.
- (14) Further comments and references on the current sensitivity of flow cytometry are provided in the Supporting Information.
- (15) Gold nanoparticles (with 31 000 atoms in a 10 nm diameter particle) are not suitable because Au, with a high ionization potential (9.7 eV), is not fully ionized in the plasma. More troubling is that it suffers background from memory effects on the sample introduction system.
- (16) Alivisatos, A. P. Semiconductor Clusters, Nanocrystals, and Quantum Dots. *Science* **1996**, *271*, 933–937.
- (17) Shen, J.; Sun, L.-D.; Yan, C.-H. Luminescent Rare Earth Nanomaterials for Bioprobe Applications. *Dalton Trans.* **2008**, 5687–5697.
- (18) Hifumi, H.; Yamaoka, S.; Tanimoto, A.; Citterio, D.; Suzuki, K. Gadolinium-Based Hybrid Nanoparticles as a Positive MR Contrast Agent. *J. Am. Chem. Soc.* **2006**, *128*, 15090–15091.
- (19) Tong, S.; Hou, S.; Ren, B.; Zheng, Z.; Bao, G. Self-Assembly of Phospholipid–PEG Coating on Nanoparticles through Dual Solvent Exchange. *Nano Lett.* **2011**, *11*, 3720–3726.
- (20) Chattopadhyay, P. K.; Gaylord, B.; Palmer, A.; Jiang, N.; Raven, M. A.; Lewis, G.; Reuter, M. A.; Nur-ur Rahman, A. K. M.; Price, D. A.; Betts, M. R.; Roederer, M. Brilliant Violet Fluorophores: A New Class of Ultrabright Fluorescent Compounds for Immunofluorescence Experiments. *Cytometry, Part A* **2012**, *81A*, 456–466.
- (21) Chattopadhyay, P. K.; Price, D. A.; Harper, T. F.; Betts, M. R.; Yu, J.; Gostick, E.; Perfetto, S. P.; Goepfert, P.; Koup, R. A.; De Rosa, S. C.; Bruchez, M. P.; Roederer, M. Quantum Dot Semiconductor Nanocrystals for Immunophenotyping by Polychromatic Flow Cytometry. *Nat. Med.* **2006**, *12*, 972–977.
- (22) Ferrari, B. C.; Bergquist, P. L. Quantum Dots as Alternatives to Organic Fluorophores for *Cryptosporidium* Detection Using Conventional Flow Cytometry and Specific Monoclonal Antibodies: Lessons Learned. *Cytometry, Part A* **2007**, *71A*, 265–271.
- (23) Zhang, X.; Yang, S. Nonspecific Adsorption of Charged Quantum Dots on Supported Zwitterionic Lipid Bilayers: Real-Time Monitoring by Quartz Crystal Microbalance with Dissipation. *Langmuir* **2011**, *27*, 2528–2535.
- (24) Li, Z. Q.; Zhang, Y. An Efficient and User-Friendly Method for the Synthesis of Hexagonal-Phase NaYF₄:Yb, Er/Tm Nanocrystals with Controllable Shape and Upconversion Fluorescence. *Nanotechnology* **2008**, *19*, 345606.
- (25) Qian, H. S.; Zhang, Y. Synthesis of Hexagonal-Phase Core–Shell NaYF₄ Nanocrystals with Tunable Upconversion Fluorescence. *Langmuir* **2008**, *24*, 12123–12125.
- (26) Johnson, N. J. J.; Korinek, A.; Dong, C.; van Veggel, F. C. J. M. Self-Focusing by Ostwald Ripening: A Strategy for Layer-by-Layer Epitaxial Growth on Upconverting Nanocrystals. *J. Am. Chem. Soc.* **2012**, *134*, 11068–11071.
- (27) (a) Johnson, B.; Prudhomme, R. Flash Nanoprecipitation of Organic Actives and Block Copolymers Using a Confined Impinging Jets Mixer. *Aust. J. Chem.* **2003**, *21*, 1021–1024. (b) Shan, J.; Budijono, S. J.; Hu, G.; Yao, N.; Kang, Y.; Ju, Y.; Prud'homme, R. K. Pegylated Composite Nanoparticles Containing Upconverting Phosphors and *meso*-Tetraphenyl porphine (TPP) for Photodynamic Therapy. *Adv. Funct. Mater.* **2011**, *21*, 2488–2495.
- (28) Hou, Y.; Qiao, R.; Fang, F.; Wang, X.; Dong, C.; Liu, K.; Liu, C.; Liu, Z.; Lei, H.; Wang, F.; Gao, M. NaGdF₄ Nanoparticle-Based Molecular Probes for Magnetic Resonance Imaging of Intraperitoneal Tumor Xenografts in Vivo. *ACS Nano* **2013**, *7*, 330–338.
- (29) Cao, P.; Hou, Y.; Tong, L.; Zhao, G.; Guerin, G.; Winnik, M. A.; Nitz, M. Improving Lanthanide Nanocrystals Colloidal Stability in Competitive Aqueous Buffer Solutions Using Multivalent PEG-Phosphonate Ligands. *Langmuir* **2012**, *28*, 12861–12870.
- (30) Jiang, G. C.; Pichaandi, J.; Johnson, N. J. J.; Burke, R. D.; van Veggel, F. C. J. M. An Effective Polymer Cross-Linking Strategy To Obtain Stable Dispersions of Upconverting NaYF₄ Nanoparticles in

Buffers and Biological Growth Media for Biolabeling Applications. *Langmuir* **2012**, *28*, 3239–3247.

(31) Ornatsky, O. I.; Lou, X.; Nitz, M.; Schafer, S.; Sheldrick, W. S.; Baranov, V. I.; Bandura, D. R.; Tanner, S. D. Study of Cell Antigens and Intracellular DNA by Identification of Element-Containing Labels and Metallointercalators Using Inductively Coupled Plasma Mass Spectrometry. *Anal. Chem.* **2008**, *80*, 2539–2547.

(32) Fiddes, L. K.; Chan, H. K. C.; Wyss, K.; Simmons, C. A.; Kumacheva, E.; Wheeler, A. R. Augmenting Microgel Flow via Receptor-Ligand Binding in the Constrained Geometries of Microchannels. *Lab Chip* **2009**, *9*, 286–290.

(33) Chen, K.; Merkel, T. J.; Pandya, A.; Napier, M. E.; Luft, J. C.; Daniel, W.; Sheiko, S.; DeSimone, J. M. Low Modulus Biomimetic Microgel Particles with High Loading of Hemoglobin. *Biomacromolecules* **2012**, *13*, 2748–2759.

(34) Lee, S.; Hoshino, Y.; Randall, A.; Zeng, Z.; Baldi, P.; Doong, R.; Shea, K. J. Engineered Synthetic Polymer Nanoparticles as IgG Affinity Ligands. *J. Am. Chem. Soc.* **2012**, *134*, 15765–15772.

(35) Lin, W.; Ma, X.; Qian, J.; Abdelrahman, A. I.; Halupa, A.; Baranov, V.; Pich, A.; Winnik, M. A. Synthesis and Mass Cytometric Analysis of Lanthanide-Encoded Polyelectrolyte Microgels. *Langmuir* **2011**, *27*, 7265–7275.

(36) Hoare, T.; Pelton, R. Titrametric Characterization of pH-Induced Phase Transitions in Functionalized Microgels. *Langmuir* **2006**, *22*, 7342–7350.

(37) Ponratnam, S.; Kapur, S. L. Reactivity Ratios of Ionizing Monomers in Aqueous Solution. Copolymerization of Acrylic and Methacrylic Acids with Acrylamide. *Makromol. Chem.* **1977**, *178*, 1029–1038.

(38) Green, N. M. Avidin. *Adv. Protein Chem.* **1975**, *29*, 85–133.

(39) Squire, P. G.; Moser, P.; O'Konski, C. T. The Hydrodynamic Properties of Bovine Serum Albumin Monomer and Dimer. *Biochemistry* **1968**, *7*, 4261–4272.

(40) Gruner, G. Carbon Nanotube Transistors for Biosensing Applications. *Anal. Bioanal. Chem.* **2006**, *384*, 322–335.

(41) Lu, Y.; Chau, M.; Boyle, A. J.; Liu, P.; Niehoff, A.; Weinrich, D.; Reilly, R. M.; Winnik, M. A. Effect of Pendant Group Structure on the Hydrolytic Stability of Polyaspartamide Polymers under Physiological Conditions. *Biomacromolecules* **2012**, *13* (5), 1296–1306.

(42) Shen, J.; Sun, L.; Zhang, Y.; Yan, C. Superparamagnetic and Upconversion Emitting $\text{Fe}_3\text{O}_4/\text{NaYF}_4:\text{Yb},\text{Er}$ Hetero-Nanoparticles via a Crosslinker Anchoring Strategy. *Chem. Commun.* **2010**, *46*, 5731–5733.